Identification of a Membrane-Spanning Domain of the Thiol-Activated Pore-Forming Toxin *Clostridium perfringens* Perfringolysin O: An α-Helical to β-Sheet Transition Identified by Fluorescence Spectroscopy†

Laura A. Shepard,‡ Alejandro P. Heuck,§ Brian D. Hamman,§,|| Jamie Rossjohn,⊥ Michael W. Parker,⊥ Kathleen R. Ryan,§,@ Arthur E. Johnson,*,§,$,# and Rodney K. Tweten*,‡

Department of Microbiology and Immunology, The University of Oklahoma Health Sciences Center, Oklahoma City, Oklahoma 73190, Department of Medical Biochemistry & Genetics, Department of Chemistry, and Department of Biochemistry and Biophysics, Texas A&M University, College Station, Texas 77843-1114, and The Ian Potter Foundation Protein Crystallography Laboratory, St. Vincent's Institute of Medical Research, Fitzroy, Victoria 3065, Australia

Received June 18, 1998; Revised Manuscript Received August 19, 1998

ABSTRACT: *Clostridium perfringens* perfringolysin O (PFO or θ-toxin) is a cytolytic toxin that binds to cholesterol-containing membranes and then self-associates to spontaneously form aqueous pores of varying size in the bilayer. In this study, a membrane-spanning domain has been identified in PFO by a combination of fluorescence spectroscopic methods using the fluorescent dye *N*,*N*′-dimethyl-*N*-(iodoacetyl)-*N*′-(7-nitrobenz-2-oxa-1,3-diazolyl)ethylenediamine (NBD) whose emission properties are sensitive to water. PFO was substituted with a single cysteine at most of the residues between amino acids K189 and N218, and then each cysteine was modified with NBD. Each purified NBD-labeled PFO was then bound to membranes, and the probe's environment was ascertained by measuring its fluorescence lifetime, emission intensity, and collisional quenching with either aqueous (iodide ions) or nonaqueous (nitroxide-labeled phospholipids) quenchers. Lifetime and intensity measurements revealed that the amino acid side chains in this region of the membrane-bound PFO polypeptide alternated between being in an aqueous or a nonaqueous environment. This pattern indicates that this portion of the membrane-bound PFO spans the membrane in an antiparallel β-sheet conformation. The alternating exposure of these residues to the hydrophobic interior of the bilayer was demonstrated by their susceptibility to quenching by nitroxide moieties attached to phospholipid acyl chains. Residues K189−N218 therefore form a two-stranded, amphipathic β-sheet in the membrane-bound PFO that creates a stable interface between the pore and the membrane. This same region packs as three short α-helices in the soluble, monomeric form of PFO, and therefore, the cholesterol-dependent conversion of PFO to a membrane-bound oligomer involves a major structural transition in which three α-helices unfold to form a membrane-spanning amphipathic β-sheet.

The "thiol-activated" bacterial toxins represent a large family of oligomerizing, cytolytic toxins that are produced by a variety of Gram-positive bacteria, including species within the genera *Clostridium*, *Streptococcus*, *Listeria*, and *Bacillus* (reviewed in ref. *1*). The most recently identified family member was detected in *Arcanobacterium* (*Actinomyces*) *pyogenes* (*2*). The members of this toxin family exhibit 40−80% identity at the primary structure level, so it is likely that many of the mechanistic features of these toxins will be similar. These toxins exhibit several unique features, including the absolute requirement for cholesterol in the membrane for cytolytic activity and, with the exception of the *A. pyogenes* toxin, the presence of a single cysteine at a structurally sensitive and highly conserved site. The thiol-activated cytolysins disrupt the membrane of target cells by forming a large homo-oligomeric structure, estimated to contain approximately 50 toxin monomers, that creates a hole up to 150 Å in diameter in the membrane (*3*).

Although there is a plethora of data on these proteins, many features of the cytolytic mechanism of these toxins remain unknown. One of the most important unknowns is which portion of the water-soluble toxin monomer is inserted into the phospholipid bilayer in the oligomeric complex. The

† These studies were supported by a grant to R.K.T. from the National Institutes of Health (AI37657), the Robert A. Welch Foundation (A.E.J.), and a National Science Foundation fellowship (GRE0355771) to L.A.S.

* Corresponding authors. R.K.T.: Department of Microbiology and Immunology, BMSB, Rm 1053, 940 Stanton L. Young Blvd., The University of Oklahoma Health Sciences Center, Oklahoma City, OK 73190; phone, (405) 271-2133; fax, (405) 271-3117; e-mail, Rod-Tweten@ouhsc.edu. A.E.J.: Department of Medical Biochemistry & Genetics, Texas A&M University Health Science Center, College Station, TX 77843-1114; phone, (409) 862-3188; fax, (409) 862-3339; e-mail, aejohnson@tamu.edu.

‡ Department of Microbiology and Immunology, The University of Oklahoma Health Sciences Center.

§ Department of Medical Biochemistry & Genetics, Texas A&M University.

|| Current address: Aurora Biosciences Corp., 11010 Torreyana Rd., La Jolla, CA 92121.

⊥ St. Vincent's Institute of Medical Research.

@ Current address: Department of Developmental Biology, Stanford University, Palo Alto, CA 94305.

$ Department of Chemistry, Texas A&M University.

Department of Biochemistry and Biophysics, Texas A&M University.

S0006-2960(98)01452-4 CCC: $15.00
Published on Web 09/25/1998

recently solved structure of the perfringolysin O (PFO) monomer (*4*) provides a useful starting point for designing studies to determine the membrane-inserted domains of PFO and for identifying the structural changes that occur during the transition of PFO from a soluble monomer to a membrane-bound complex. The formation of a pore by oligomerized PFO requires the PFO polypeptide within the bilayer to have an amphipathic character, with the hydrophilic side of this domain facing the aqueous pore and the hydrophobic side facing and interacting with the nonpolar core of the phospholipid bilayer. Amphipathic α-helix (*5*) and β-sheet (*6*) structures have both been observed previously in bacterial toxins to form aqueous channels in membranes, and it has been suggested recently that streptolysin O (SLO), a toxin whose sequence is approximately 65% homologous to that of PFO, may interact with the membrane of target cells via a pair of amphipathic α-helices, a conclusion based on cysteine-scanning mutagenesis and the use of the fluorescent dye acrylodan[1] (*7*).

If the transmembrane domain(s) of PFO assumes an α-helical or a β-sheet structure, then one can identify the conformation that is present by examining the periodicity of the environment of the amino acid side chains in the membrane-bound PFO. In this study, we have used the combined data from several fluorescence spectroscopic techniques to show that a membrane-interactive domain of PFO forms an amphipathic antiparallel β-sheet structure. Furthermore, sequence comparisons of the thiol-activated toxins suggest that the formation of an extended β-sheet is a common structural rearrangement that accompanies toxin oligomerization and insertion for this large family of toxins.

EXPERIMENTAL PROCEDURES

Bacterial Strains, Plasmids, and Chemicals. The gene for PFO^{C459A} (cysteine-less derivative of PFO in which Cys459 was replaced by Ala) was cloned into pTrcHisA (Invitrogen, Carlsbad, CA) via the *Bam*HI and *Eco*RI sites of the vector. The codon for S28 of PFO was fused to the polyhistidine tag of the pTrcHisA vector at the *Bam*HI site and the termination codon of the PFO gene was fused at the 3′ end to the *Eco*RI site of the vector. PFO was expressed intracellularly from this vector (designated pRT20) in *Escherichia coli* strain XL-1 Blue (Novagen, Madison, WI) and contained the polyhistidine tag and enterokinase cleavage site at its amino terminus. The *pfu* thermostable polymerase (Stratagene, La Jolla, CA) was used for all PCR amplifications due to its low error rate. DNA sequencing was carried out by personnel of the Department of Microbiology and Immunology Automated DNA Sequencing Core Facility at the University of Oklahoma Health Sciences Center. All phospholipids were obtained from Avanti Polar Lipids (Alabaster, AL), and cholesterol was obtained from Steraloids (Wilton, NH). All chemicals and enzymes were obtained from Sigma Chemical Co. (St. Louis, MO) unless otherwise specified.

[1] Abbreviations: iodoacetamide-NBD or IANBD, *N*,*N*′-dimethyl-*N*-(iodoacetyl)-*N*′-(7-nitrobenz-2-oxa-1,3-diazolyl)ethylenediamine; acrylodan, 6-acryloyl-2-(dimethylamino)naphthalene. PFO^{A215C} is an example of the notation for the cysteine-substituted mutants. The superscript text indicates that this derivative of the cysteine-less parent toxin, PFO^{C459A}, has A215 substituted with a cysteine. If it is designated $NBD-PFO^{A215C}$, then the cysteine has been derivatized with iodoacetamide-NBD.

PCR Mutagenesis of the PFO^{C459A} Gene. All cysteine substitutions were generated using pRT20 (expressing PFO^{C459A}) DNA as the template for PCR overlap mutagenesis as described by Ho et al. (*8*) except that *pfu* polymerase was substituted for *taq* polymerase. The PCR overlap products were extracted with phenol, digested with *Bam*HI and *Eco*RI, and ligated into *Bam*HI- and *Eco*RI-digested pTrcHisA.

Expression and Purification of PFO. Expression and purification of PFO containing an amino-terminal hexahistidine tag were carried out as follows. Growth of *E. coli* XL-1 Blue containing pRT20 or derivatives thereof was initiated by inoculating one 8 L container of sterile TB broth (*9*) (containing 200 μg/mL ampicillin and 1 mL of sterile anti-foam) with a 1:33 inoculum of an overnight culture grown at 30 °C. The 8 L culture was incubated at 37 °C with constant aeration by sterile-filtered air introduced through an air dispersion tube. Expression of PFO was induced by the addition of isopropyl β-D-thiogalactopyranoside (IPTG, Gold Biochemicals, St. Louis, MO) to a final concentration of 1 mM when the A_{600nm} of the culture reached 1.0. The induced culture was grown for 4 h, and the cells were harvested by centrifugation.

The cell pellets from an 8 L culture were suspended in a total of 160 mL of 10 mM MES [2-(*N*-morpholino)-ethanesulfonic acid] (Research Organics, Cleveland, OH) and 150 mM NaCl at pH 6.5 (buffer A). The cells were lysed by one passage through a French pressure cell (1 in. diameter piston, Aminco, Silverspring, MD) at 20 000 psi. The cell debris was removed by centrifugation at 30000*g* for 15 min at 4 °C. The PFO-containing supernatant was loaded onto a column (1.5 cm inside diameter × 10 cm) containing Chelating Sepharose Fast Flow (Pharmacia, Piscataway, NJ) that had been preloaded with Co^{2+} and equilibrated with buffer A at room temperature. The polyhistidine-tagged PFO bound to this resin, while most other proteins passed through without binding. The column was washed (2 mL/min) with 130 mL of buffer A to remove additional contaminating proteins. The bound PFO was eluted (2 mL/min) with 100 mL of buffer A containing 300 mM imidazole. The fractions containing the bulk of the hemolytic activity were pooled, diluted 3-fold with buffer B [10 mM MES (pH 6.5) containing 1 mM EDTA], and loaded directly onto a column (1.5 cm inside diameter × 10 cm) packed with the cation exchange resin SP Sepharose HP (Pharmacia) equilibrated in buffer B. The column was eluted with a 315 mL linear gradient (3 mL/min) from 0 to 1 M NaCl in buffer B with PFO eluting at approximately 0.5 M NaCl. The fractions which contained the PFO were pooled, made 10% (v/v) in glycerol and 5 mM in dithiothreitol (DTT), aliquoted into cryovials, and quick-frozen in liquid nitrogen. The samples were stored at −80 °C. All chromatography was performed with a Rainin titanium high-pressure liquid chromatography system (Woburn, MA) and Dynamax software. The protein was quantified by absorbance at 280 nm using a molar extinction coefficient for PFO of 84 000 M^{-1} cm^{-1} (R. K. Tweten, unpublished data).

Modification of Cysteine-Substituted PFO with IANBD. In a typical labeling reaction, 2 mg (1−2 mg/mL) of a cysteine-substituted PFO derivative was thawed and passed over a column (1.5 cm inside diameter × 20 cm) containing Sephadex G-50 [equilibrated in 50 mM HEPES (pH 8.0), 100 mM NaCl, and 1 mM EDTA] at room temperature to

remove the excess DTT. The eluted toxin was concentrated to approximately 0.5−1 mg/mL using an Amicon model 8010 ultrafiltration cell (Amicon, Danvers, MA) (equipped with a 10 kDa molecular mass cutoff membrane), and crystalline guanidine hydrochloride was added to 3 M. IANBD (Molecular Probes, Eugene, OR) was then added to a concentration that provided a 10-fold molar excess of reagent over the PFO. After 2 h at room temperature (22 °C), the reaction was quenched by the addition of DTT to 5 mM and the mixture passed over a 1.5 cm inside diameter × 20 cm column containing Sephadex G-50 equilibrated in buffer C [50 mM HEPES (pH 7.5) and 100 mM NaCl]. The fractions containing the NBD-labeled toxin were pooled, made 10% (v/v) in glycerol, aliquoted, quick-frozen in liquid nitrogen, and stored at −80 °C until they were used. The extent of covalent reaction with NBD was estimated using an ϵ_{478nm} of 25 000 M^{-1} cm^{-1} for NBD (*10*).

Hemolytic Titration. The hemolytic activities of all NBD-labeled and unlabeled proteins were determined as follows. Washed human erythrocytes were suspended in PBS [10 mM Na_2HPO_4 (pH 7.4) containing 147 mM NaCl and 3 mM KCl]- to 10 vol %. One milliliter of the erythrocyte suspension was then treated with 0.18 pmol of mutant or native PFO and incubated at 37 °C for 30 min in parallel with controls containing either no PFO (0% lysis control) or excess (1.8 pmol) native PFO (100% lysis control). After incubation, any unlysed erythrocytes were removed from the samples by centrifugation at 13000*g* for 30s. The extent of hemoglobin release was quantified by measuring the A_{540nm} of the supernatant using a DU640B spectrophotometer (Beckman). The activity of 0.18 pmol of each mutant PFO was expressed as a percentage of the hemolytic activity of 0.18 pmol of PFO^{C459A}.

Liposome and Erythrocyte Ghost Membrane Preparation. Large unilamellar liposomes were generated using an Avestin Inc. (Ottawa, ON) Liposofast extruder and polycarbonate membranes with a 100 nm pore size (*11*). A mixture (55: 45 mol %) of cholesterol (15.5 mg) and egg lecithin (25 mg) or of cholesterol (8.5 mg) and 1-palmitoyl-2-oleoyl-*sn*-glycero-3-phosphocholine (POPC) (13.6 mg) in chloroform was dried under a stream of argon or nitrogen at 40 °C and then dried further under vacuum for an additional 3 h. The dried phospholipid/sterol mixture was suspended in 3 mL of buffer C by vortexing and then was sonicated in a water bath for 5 min to ensure that the lipid was fully hydrated. The suspended phospholipid/sterol mixture was then passed (0.5 mL at a time) 21 times through the liposome extruder to generate the liposomes. The liposomes were stored under argon or nitrogen at 4 °C and used within 5 days of production. Liposomes used in lipophilic quenching experiments were prepared using POPC and cholesterol as above, except that 10, 20, or 30 mol % of the POPC was replaced by the nitroxide-labeled phospholipid [1-palmitoyl-2-stearoyl-(7-doxyl)-*sn*-glycero-3-phosphocholine].

Erythrocyte ghost membranes were prepared as described previously (*12*) and were used at a concentration of approximately 5×10^7 ghost membranes/mL.

Steady-State Fluorescence Spectroscopy. Steady-state fluorescence measurements were taken using an SLM 8100 photon-counting spectrofluorimeter with a double monochromator in the excitation light path, a single emission monochromator, cooled PMT housings, and a 450 W xenon lamp (Spectronic Instruments, Rochester, NY). The emission wavelength was 530 nm, and the excitation wavelength was either 468 or 470 nm; the band-pass was typically 4 nm. In each case, the net NBD intensity was determined by subtracting the signal of an equivalent NBD-free sample prepared with unmodified PFO. Emission scans of both monomeric and oligomeric forms of each mutant were carried out at 1 nm intervals between 500 and 600 nm. An emission spectrum of a sample lacking NBD was subtracted from the spectrum of the equivalent sample containing NBD. Most intensity measurements were taken at 25 °C in buffer C in 1 cm × 1 cm quartz cuvettes; nitroxide quenching experiments were carried out at 20 °C using 4 mm × 4 mm quartz microcells that were coated with dioleoylphosphatidylcholine vesicles to minimize adsorption (*13*). When excess liposomes (determined by titration) were added to a sample of monomeric NBD-labeled PFO, the resulting sample was incubated at 37 °C for 10 min to allow oligomerization and insertion of PFO into the bilayer to go to completion, and then cooled for 5 min to 25 °C before the intensity was measured again. When additions were made to microcells, the contents were mixed thoroughly with a 2 mm × 2 mm magnetic stirring bar as described previously (*14*), whereas samples were stirred continuously in the larger cuvettes. Since the same results were obtained with the larger and smaller cuvettes, the above differences in sample handling did not affect our conclusions.

Fluorescence Lifetimes. Time-resolved fluorescence measurements were taken using an ISS (Urbana, IL) K2-002 multifrequency cross-correlation phase and modulation spectrofluorimeter equipped with a digital filter and fast Fourier transform data acquisition. Samples of 100−600 nM NBD-labeled PFO derivatives, either with or without excess liposomes prepared as described above, were excited in 1 cm × 1 cm quartz cuvettes at 25 °C in buffer C using the 457.9 nm line of a Coherent (Santa Clara, CA) Innova 400-15/4 argon ion laser, and fluorescence emission was collected through an Oriel OG-515 filter. Polarization artifacts were avoided by passing the exciting light through a vertically oriented Glan-Taylor polarizer and collecting the emission through a Glan-Thompson polarizer oriented at an angle of 55° relative to the vertical laboratory axis (*15*). Since the background signal, including Raman and Rayleigh scattering, was always less than 10% even with liposomes, no blank subtraction was done to correct for background emission and scattering. Either disodium fluorescein in 0.1 M KOH (τ = 4.05 ns) or scattered light from glycogen in water was used to standardize the instrument.

Phase and modulation data were analyzed using GLOBALS UNLIMITED, obtained from the University of Illinois (Urbana, IL). Data were fit to decay models involving one or more exponentials, or one exponential and one or two Lorentzian distributions of decay processes. The latter functional form introduces an additional parameter, corresponding to the width of the distribution, to the normal parameters of lifetime and fractional contribution of each component (*16*). In each case, the lowest χ^2 value was obtained with a two-component fit consisting of a single exponential with a τ of 0.001 ns to correct for scatter and a single Lorentzian distribution for the NBD emission lifetime; fitting the data to multiple exponentials and/or Lorentizians did not significantly improve the χ^2. The fractional contribu-

tion of the scattering determined by this analysis corresponded closely to the fraction of total signal intensity that resulted from Raman and Rayleigh scattering.

Collisional Quenching of NBD Emission Intensity by Iodide Ions. Two equivalent NBD-containing samples in buffer C at 25 °C were titrated in parallel, one with 1 M KI and 1 mM $Na_2S_2O_3$ and the other with 1 M KCl and 1 mM $Na_2S_2O_3$, as were two control samples lacking NBD. The initial net (after the signal of the control sample had been subtracted) fluorescence intensity (F_o) was determined for each monomeric or membrane-bound NBD−PFO sample prior to the addition of any KCl or KI, and the emission intensities of each sample and its control were then measured after each addition and dilution-corrected to obtain the net emission intensity (F). In these experiments, the net change in fluorescence due to iodide ion quenching at each KI/KCl concentration was given by the equation $F_o/F = (F_o/F)_{KI}/(F_o/F)_{KCl}$.

For collisional quenching of fluorescence, a linear plot is obtained when the data are analyzed according to the Stern−Volmer law:

$$(F_o/F) - 1 = K_{sv}[I^-] \quad (1)$$

where F_o is the net emission intensity in the absence of quencher, F is the net emission intensity in the presence of I^-, and K_{sv} is the Stern−Volmer quenching constant. K_{sv} is equal to $k_q\tau_o$, where k_q is the bimolecular quenching constant and τ_o is the fluorescence lifetime in the absence of quencher. The k_q values reported below were determined by a linear least-squares analysis of the combined data from two independent experiments.

Quenching of NBD Emission Intensity by Spin-Labeled Phospholipids. The emission intensities of four 100 nM aliquots of a monomeric NBD−PFO sample in buffer C were measured at 20 °C, and then excess liposomes containing 0, 10, 20, or 30 mol % of the nitroxide-modified phospholipid were added to each sample to a final concentration of 50 μM. After incubation at 37 °C for 40 min, the samples were returned to 20 °C, and their intensities were redetermined. These intensities were normalized to account for differences in the NBD−PFO content in each sample. To calculate F_o/F, F_o was the oligomer intensity in the nitroxide-free sample and F was the oligomer intensity in the sample containing 20 mol % of the nitroxide-labeled phospholipid.

RESULTS

Experimental Strategy. When PFO and related toxins interact with the membrane, they form a boundary between the lipid bilayer and an aqueous pore that is large enough that macromolecules pass through it. A portion of the PFO polypeptide will span the bilayer and form the interface between the aqueous channel and the nonpolar core of the bilayer. If the PFO polypeptide spans the membrane in a β-sheet conformation, as does α-hemolysin (*6*), then one would expect the environment of residues along the membrane-bound polypeptide to alternate between aqueous (facing the pore) and nonpolar (facing the core of the bilayer). Alternatively, if the PFO inserts into the bilayer as an amphipathic α-helix, as proposed for SLO (*7*), then the residues facing the aqueous pore or the nonpolar bilayer can be predicted by a helical wheel analysis of the residues in the α-helix.

To directly determine the environment of a particular amino acid side chain in PFO, that residue is replaced by a cysteine and a fluorescent dye is then covalently attached to the sulfhydryl group of the newly introduced cysteine. The fluorescently labeled PFO is then bound to and inserted into a membrane, and its spectral properties are examined. Many fluorescent dyes are sensitive to the presence of water, and their emission properties change dramatically upon moving from an aqueous to a nonaqueous milieu. NBD was chosen as the fluorescent probe in this study because its emission intensity and lifetime both increase substantially upon moving from an aqueous solvent into the nonpolar core of the bilayer (*17*, *18*). Moreover, NBD has a relatively small size for a dye; it is uncharged, and its N and O atoms give the dye sufficient polar character to be soluble in an aqueous environment. The last property is important because the dye should serve as a stable reporter group in both aqueous and nonaqueous environments. The dye should not be so hydrophobic that it buries itself in the bilayer irrespective of the conformation of the native unmodified polypeptide, as is sometimes seen with a highly hydrophobic dye such as acrylodan (*19*).

In contrast to the proposed α-helical transmembrane domain for SLO (*7*), inspection of the primary structure of PFO suggested the presence of a region extending from residue 189 to 218 that exhibited the characteristics of a membrane-spanning amphipathic β-sheet structure (Figure 1). Furthermore, when the primary structures of the other known thiol-activated toxins were aligned with the PFO sequence, these related toxins all exhibited a pattern consistent with an amphipathic β-sheet structure in the same location that was long enough to span a single bilayer (Figure 1). In all cases, these toxins exhibited a core of residues that approximately corresponded to residues Q191−A213 of PFO that could potentially form a two-stranded, amphipathic β-sheet. Although some of these related toxins did not have β-strands as long as that identified in the PFO structure, they all had at least 10 residues per strand that exhibited the amphipathic characteristic. The minimum length of a β-sheet necessary to cross a bilayer is eight or nine amino acids (*20*). The conserved nature of this region strongly suggested the presence of a transmembrane amphipathic β-sheet in PFO and the other related toxins.

The amino acid residues of the putative transmembrane region were therefore targeted by cysteine substitution into a cysteine-less derivative of PFO in which the only native cysteine, C459, had been replaced with alanine to yield PFO^{C459A}. The alanine substitution for C459 did not significantly affect the hemolytic activity of PFO (R. K. Tweten, unpublished data). Similar results have been reported for the related toxins pneumolysin (*21*) and streptolysin O (*22*) when the corresponding cysteine was replaced with alanine. Unique cysteines were then substituted for the residues in the suspected amphipathic region of PFO^{C459A} and were used for the site-specific attachment of the fluorescent probe NBD.

Hemolytic Activity of the NBD-Labeled PFO Mutants. The PFO derivatives harboring the cysteine substitutions within this region typically retained >80% of the activity of PFO^{C459A} (Table 1). The exceptions were PFO^{V209C} and PFO^{A213C} which retained less than 30% of the hemolytic activity of PFO^{C459A}. The reduced activity of PFO^{V209C} may

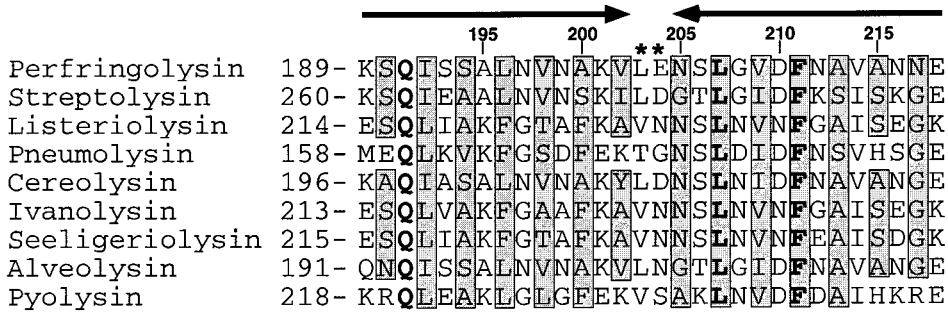

FIGURE 1: Possible amphipathic β-sheet structure in PFO and related toxins. The primary structure of PFO was aligned with the primary structures of other sequenced thiol-activated toxins. The arrows indicate the location of the hypothesized dual-stranded, amphipathic β-sheet in PFO. The shaded residues are predicted to face the membrane, and the unshaded residues are predicted to face the channel. All of the related toxins shown contain a similar amphipathic structure in this region that varies in length from 23 residues for pyolysin to 30 residues for PFO. Although in some cases the length of the two amphipathic β-sheets may be shorter than that predicted for PFO, there is still a sufficient number of residues in each strand to span a bilayer. The asterisks indicate the proposed location where the antiparallel β-sheet folds back on itself in PFO. The numbers above the PFO sequence are the amino acid numbers for PFO.

Table 1: Relative Hemolytic Activity of Cysteine-Substituted Mutants of PFO before and after Derivatization with IANBD

PFO mutant	hemolytic activity (% of PFO^{C459A}) unlabeled	NBD-labeled	PFO mutant	hemolytic activity (% of PFO^{C459A}) unlabeled	NBD-labeled
C459A	100		E204C	97	74
K189C	100	93	N205C	88	93
S190C			S206C	85	93
Q191C	104	91	L207C	99	43
I192C	101	<1	G208C		
S193C	88	76	V209C	25	12
S194C	82	84	D210C	96	54
A195C	100	96	F211C	77	23
L196C	101	57	N212C	103	77
N197C	90	60	A213C	28	59
V198C	101	52	V214C	98	51
N199C	98	82	A215C	92	95
A200C			N216C	99	85
K201C	99	95	N217C	100	105
V202C	100	62	E218C	101	99
L203C	100	40			

result from its tendency to precipitate easily during and after purification, a property that prevented us from characterizing this mutant spectroscopically. For reasons unknown, cysteine substitution of residues S190, A200, and G208 was not achieved by PCR mutagenesis after multiple attempts to generate these mutants.

The cysteine-substituted PFO mutants were labeled with IANBD with a 90−100% efficiency. The hemolytic activity of most of the NBD-labeled species was >50% of PFO^{C459A}, thereby suggesting that the NBD-labeled molecules were generally less active than their underivatized counterparts. The decreased hemolytic activity was not due to the labeled molecules being unable to bind to membranes, since the magnitude of the membrane-dependent increase in tryptophan emission intensity, previously shown to accompany PFO binding to membranes (*23*), was the same for PFO^{C459A} and each of the NBD-labeled mutants (data not shown). The fluorescence lifetime data (see below) also reveal that, in every case, all of the NBD dyes in a membrane-bound NBD−PFO sample were in the same environment. Thus, we observed no samples in which the proteins appeared to be split between soluble and membrane-bound forms which would have been suggestive of a pool of PFO molecules incapable of insertion. For example, all of the NBD dyes in a sample of NBD−PFO^{V214C} moved from a relatively hydrophobic ($\tau = 4$ ns) environment into a polar environment when exposed to liposomes ($\tau = 1$ ns), even though it was only 51% as active as the parent toxin. Thus, this protein was fully bound to membranes, even though its hemolytic activity was low.

These functional data suggest the existence of an intermediate state for membrane-associated PFO in which the toxin is bound to the membrane and this portion of the PFO is inserted in the bilayer, but the toxin is unable to achieve hemolysis. It therefore appears that the NBD-labeled PFO derivatives that exhibit significantly less hemolytic activity (e.g., NBD−PFO^{I192C}) may insert properly, but are unable to complete a subsequent step in the cytolytic mechanism (possibly oligomerization) due to the presence of the NBD. The extent of this effect in different mutants may depend on the extent of interaction of particular residues with the β-sheet of the adjacent monomer. Further investigation will be required to clarify what the uncoupling of hemolysis and membrane-binding observed here reveals about the cytolytic mechanism of PFO. However, the homogeneity of the spectral data of each mutant allows us to discern structural features of membrane-bound PFO despite the variation in observed hemolytic activity.

Probe Environment Detected by Emission Intensity. The emission of NBD is strongly quenched by water. Thus, NBD fluorescence intensity increases significantly when the dye moves from an aqueous to a nonaqueous environment. Each NBD−PFO mutant was examined spectroscopically for changes in the fluorescence intensity of the NBD before and after the toxin was bound to cholesterol-containing liposomal membranes. Typical emission scans are shown in Figure 2 for a pair of mutants in which an NBD-labeled cysteine was substituted for adjacent residues in the putative transmembrane amphipathic β-sheet. S194 was hypothesized to face the nonpolar membrane, whereas A195 was predicted to reside on the hydrophilic face of the β-sheet. NBD attached to cysteine substituted for S194 (NBD−PFO^{S194C}) exhibited a substantial increase in fluorescence intensity, as well as a significant blue shift in the wavelength of maximum emission intensity, after NBD−PFO^{S194C} was incubated with cholesterol-containing liposomes (Figure 2A). However, no changes in the emission spectrum of NBD−PFO^{S194C} were observed when liposomes lacking cholesterol were added (Figure 2A). Thus, residue S194 appears to move from a hydrophilic to

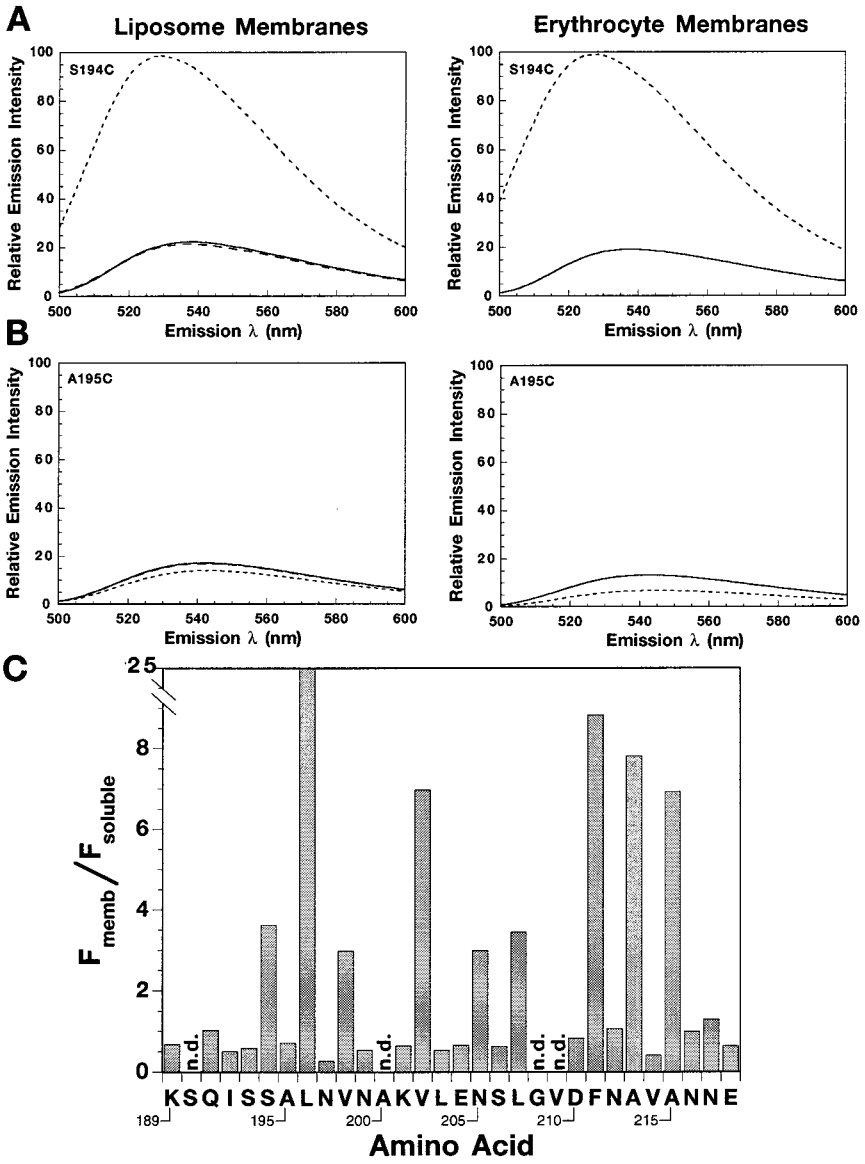

FIGURE 2: Fluorescence intensity of NBD attached to cysteine-substituted residues along a stretch of PFO predicted to be involved in membrane binding. Emission scans of the soluble monomeric and membrane-bound forms of NBD−PFO^{S194C} (A) and NBD−PFO^{A195C} (B) before and after binding to liposomes (left side) or erythrocyte ghost membranes (right side) are shown. The fluorescence emission of NBD−PFO (100 nM) was examined in buffer C (solid line), after the addition of phosphatidycholine vesicles lacking cholesterol (dashed line), or after incubation with phosphatidycholine−cholesterol vesicles (dotted line). PFO will bind and insert into the latter vesicles, but not into the cholesterol-free vesicles. The large increase in intensity upon membrane binding for the NBD located at S194 is consistent with its movement from an aqueous environment in the monomer to the nonpolar environment of the membrane. Similar results are seen in the panels on the right side in which erythrocyte ghost membranes (5×10^7/mL) were substituted for the phosphatidycholine−cholesterol vesicles. The fluorescence emission of the NBD−PFO is shown before (solid line) and after the addition of erythrocyte ghost membranes (dotted line). (C) Compilation of the NBD intensity changes ($F_{memb}/F_{soluble}$) observed at 530 nm for each residue in the putative β-sheet during the monomer ($F_{soluble}$) to membrane-bound oligomer (F_{memb}) transition with liposomes. n.d. means the values were not determined because those mutants were either unstable or not expressed. Every fifth amino acid is labeled with its primary sequence number on the *X*-axis in the bar chart in panel C.

a hydrophobic environment when PFO interacts with the membrane. As can be seen, this transition does not take place with liposomes that lack cholesterol and are comprised only of phosphatidycholine (Figure 2A). In contrast, A195 was predicted to face the hydrophilic side of the β-sheet, and consistent with that expectation, the emission intensity of NBD−PFO^{A195C} did not increase upon binding to the membrane (Figure 2B). A195 appears to be in a hydrophilic environment both before and after membrane binding. A similar response in the intensity changes for NBD−PFO^{S194C} and NBD−PFO^{A195C} was obtained if erythrocyte ghost membranes were substituted for the liposomal membranes (Figure 2A,B). The NBD−PFO spectral response is therefore the same for both natural and artificial membranes, an equivalence that is important to these analyses. The remaining analyses herein were carried out using liposomes.

When the emission intensities of membrane-bound PFO (F_{memb}) and soluble monomeric PFO ($F_{soluble}$) are compared for the residues in this region of PFO, a pattern emerges that is consistent with a membrane-interactive amphipathic β-sheet structure (Figure 2C). An alternating pattern of small or negligible intensity changes ($F_{memb}/F_{soluble} < 1.2$) and large intensity increases ($3 < F_{memb}/F_{soluble} < 25$) was observed for the NBD attached to the cysteine-substituted residues in

this region. This pattern begins at residue I192 and ends at residue N217. A turn in the antiparallel β-sheet conformation appears to occur at residues L203 and E204 since the amphipathic pattern is broken at this point, but is then re-established at amino acid N205. Thus, two amphipathic β-strands of 10−12 residues each are strongly suggested by the data to span the bilayer in membrane-bound PFO.

Emission intensity changes cannot always be used reliably to assess the location of probes following membrane binding, both because comparing the initial and final intensities can be misleading and also because the measured intensity is an average value and may obscure heterogeneity in the sample. For example, the same average intensity increase is observed if 100% of the dyes experience a 2-fold increase in intensity or if 50% of the dyes experience a 4-fold increase in intensity and the other half are unchanged. To eliminate any such uncertainty about the homogeneity of the sample, one can use time-resolved fluorescence techniques to determine directly the fluorescence lifetime of every probe in the sample. Since an NBD dye has an emission lifetime of ~1 ns in an aqueous medium and 7−8 ns when in the nonpolar core of the bilayer (*17*), lifetime analysis reveals not only the nature of the NBD environment(s) but also the sample heterogeneity (e.g., the fraction of dyes in each environment).

NBD Environment in Membrane-Bound PFO Mutants Detected by Fluorescence Lifetime. The fluorescence lifetime (τ) of NBD is sensitive to the presence of water, as noted above, and with current instrumentation, the distribution of the individual lifetimes within a sample can be determined and quantified. Thus, lifetime measurements can provide information on whether all of the NBD dyes in a sample have the same lifetime and hence are in the same environment. In this study, each mutant exhibited a single NBD lifetime in both the soluble and membrane-bound states. This was determined by analyzing the data using a variety of possibilities, including NBD dyes in one, two, or three different environments with different lifetimes, either in the presence or in the absence of light scattering. In each case, the data were best fit (i.e., had the lowest χ^2) by a single Lorentzian distribution with a small light scattering component. The lifetime results therefore indicate that all of the NBD probes in each sample were located in a common environment.

The magnitude of the NBD fluorescence lifetime in the membrane-bound NBD-labeled mutants reveals directly the environment of the dye and, in particular, its exposure to water (*17*). When the NBD fluorescence lifetime is short (0.4−2.0 ns), then the dye is in an aqueous environment. Thus, the NBD located at residues S193, A195, N197, N199, and K201 and at E204, S206, D210, N212, V214, N216, and E218 are in an aqueous milieu in the membrane-bound complex (Figure 3B). When the NBD lifetime is long (6−8 ns), then the dye is in a nonpolar milieu. Thus, NBD attached to residues S194, L196, and V198 and to L207, F211, A213, and A215 are buried in the hydrophobic core of the bilayer in the membrane-bound PFO complex (Figure 3B). In addition, several mutants had intermediate NBD fluorescence lifetimes (4−5 ns). The side chains for these residues (I192, V202, L203, N205, and N217) were clearly not in an aqueous environment, but also were not buried in the hydrophobic interior of the bilayer. Instead, the intermediate lifetimes indicate that these NBD dyes are in an

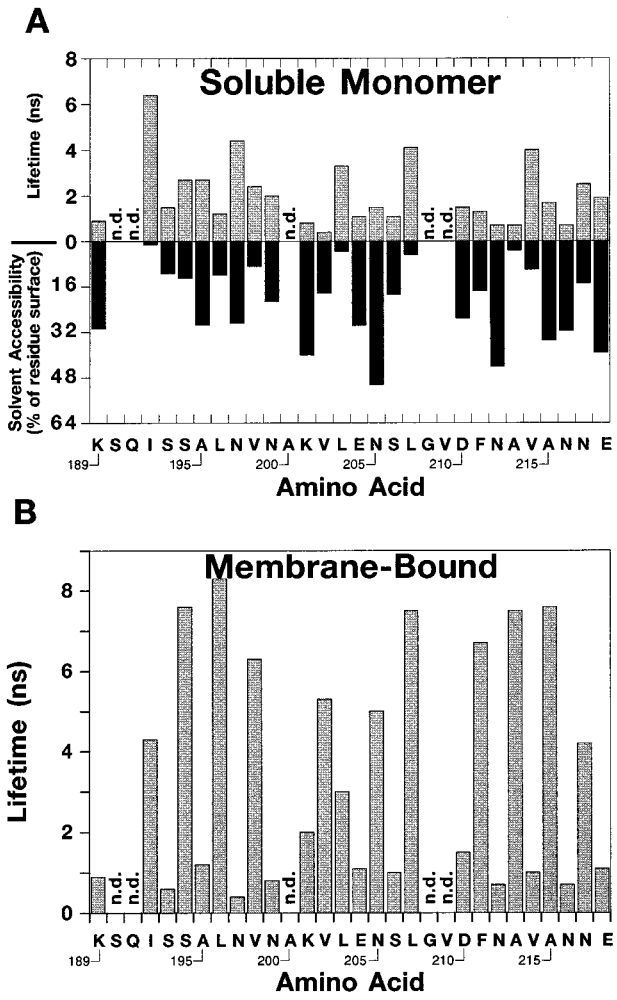

FIGURE 3: Fluorescence lifetime of NBD linked to cysteine-substituted residues along a predicted transmembrane stretch of PFO. The fluorescence lifetimes of NBD-modified cysteines that have been substituted for residues along the predicted transmembrane stretch of PFO are shown both for the soluble monomeric form of PFO (A) and for the membrane-inserted oligomeric form of PFO (B). The distribution of lifetimes in the monomer does not exhibit any specific pattern, although NBD which exhibited a longer lifetime was typically attached to residues that were less exposed to solvent, on the basis of solvent accessibility calculations using the crystal structure of monomeric PFO. However, in panel B, it is clear that once PFO inserts into the membrane an alternating pattern of short and long lifetimes for NBD emerges, depending on whether the NBD is attached to a cysteine that has been substituted for a channel-facing or membrane-facing residue of the amphipathic β-sheet. The widths of the Lorentzian distributions were 1.0 ns or less for nine mutants, 1.1−2.1 ns for ten mutants, and 2.2−2.9 ns for six mutants. n.d. means not determined. Every fifth amino acid is labeled with its primary sequence number on the *X*-axis in the bar chart in panels A and B.

environment of intermediate polarity. Hence, it is not surprising that each of these five residues is predicted to be located at an end of a transmembrane β-sheet strand and near the surface of the bilayer. When the lifetime data of the membrane-bound toxin are considered in toto, it is clear from the alternating pattern of short and long NBD lifetimes (Figure 3B) that the amino acids between residues 189 and 218 of PFO alternate between being in a hydrophilic or a hydrophobic milieu. Thus, we conclude that this portion of the PFO polypeptide extends across the membrane in an antiparallel β-sheet conformation, with one side of the sheet facing the bilayer and the other facing the aqueous pore. The

intensity data suggested the same conclusion, but not as unambiguously as the lifetime data (compare Figures 2C and 3B).

NBD Environment in Monomeric PFO. When the solvent-accessible surfaces of monomeric PFO are calculated from the crystal structure for the residues in this region, the lifetime data are in good agreement with the relative solvent accessibility of each of these residues in the monomer (Figure 3A). NBD-labeled residues I192, N197, L203, L207, and V214 all exhibit lifetimes from 3.3 to 6.4 ns and hence are relatively inaccessible to solvent in the monomer. These residues, except for N197, also have the lowest water-accessible surface area values (Figure 3A). One possible explanation for the discrepancy in the lifetime of N197 and its calculated water-accessible surface is that N197 is pointed into the interface between domains 2 and 3 of the PFO monomer. Although N197 is accessible to water, it is possible that the NBD attached to the cysteine at this site may nestle into a pocket at the domain 2−domain 3 interface and therefore may be less accessible to water. A213 is also predicted to have only 3.1% of its surface exposed to water in the monomer, yet NBD attached to the cysteine substituted at this site has a relatively short lifetime of 0.7 ns. Inspection of the monomer structure reveals that A213 actually sits near the surface of PFO, positioned in a pocket that is shielded by the side chains of D210, K219, N212, N216, and E218. It is possible that these residues shield A213 from water, while NBD attached to cysteine at this site may protrude out through these residues where its emission is quenched by water.

Collisional Quenching of Fluorescent Probes by Iodide Ions. An independent experimental approach to evaluating probe location is collisional quenching, a technique that is used to assess probe accessibility to collisional quenching agents by the magnitude, if any, of the quencher-dependent reduction in fluorescence emission. Iodide ions are efficient hydrophilic quenchers of NBD fluorescence (*17*, *18*). One would expect that all NBD probes with short lifetimes in membrane-bound PFO would be in an aqueous environment and would be quenched if I^- were added to the sample. In contrast, mutants with long NBD lifetimes would not be expected to be quenched by I^- because these probes are buried in the bilayer and are not accessible to I^-. The sensitivity of NBD emission intensity to I^- was therefore examined for each mutant.

Collisional quenching data for NBD dyes positioned at adjacent residues in PFO are shown in Figure 4A for both the soluble and the membrane-bound PFO. The linear dependence of fluorescence intensity on quencher concentration demonstrates that the quenching is collisional, as required by the Stern−Volmer expression (see Experimental Procedures), and this linearity was observed with each mutant, both monomer and membrane-bound. The extent of quenching is often given by the Stern−Volmer quenching constant (K_{sv}), which is equal to the slope of the line in the graphs on the left of Figure 4A. However, the K_{sv} values do not accurately reflect the relative collisional quenching rates if the NBD lifetimes (τ_0) differ for different species, simply because there is more time for a quencher to collide with a dye if it has a longer lifetime. The true collisional quenching frequency is determined by calculating the bimolecular quenching constant, k_q, using the relationship $k_q = K_{sv}/\tau_o$.

The importance of comparing k_q values rather than K_{sv} values is clearly evident in Figure 4A. The NBD−PFO^{L196C} data in the graph on the left indicate that the probe in membrane-bound NBD−PFO^{L196C} is only slightly less exposed to aqueous iodide ions than is the probe in the monomer as indicated by the <3-fold difference in the K_{sv} values for monomer and oligomer. However, when the data are corrected for the much longer NBD lifetime of the membrane-bound species, then the extent of collisional quenching of the buried (long lifetime) membrane-bound probe is seen to be very low (right graph of Figure 4A), with an iodide ion collisional frequency more than 18-fold lower than that of the probe in the monomer. Similarly, when the lifetimes are taken into account, it is evident that the probe in NBD−PFO^{A195C} is more exposed to I^- in the membrane-bound oligomer than in the soluble monomer, presumably because the dye is partially buried in the monomeric protein.

With the exception of K201, the k_q values for I^- quenching of the NBD-derivatized residues in membrane-bound PFO oligomers are consistent with the location of these residues in an amphipathic β-sheet (4B). Most residues that were predicted by their short fluorescent lifetimes to be facing the aqueous pore are accessible to I^- and exhibit a k_q between 5 and 11 M^{-1} ns^{-1}. Those residues facing the nonpolar core of the bilayer (NBD fluorescence lifetimes of >6 ns) have very low collisional frequencies with I^- (k_q < 1.5 M^{-1} ns^{-1}), as expected. For comparison, the k_q for the quenching of free N^{ϵ}-(NBD)-lysine is 7.9 M^{-1} ns^{-1} (*17*). The NBD probe at K201 was expected to be quenched efficiently by the iodide ions, but it was not, even though the lifetime, intensity, and nitroxide quenching data (Figures 2, 3, and 5) show that this probe is not buried in the bilayer. The NBD probe at residue K201 therefore appears to be in an environment that is accessible to water molecules, but not to the much larger iodide ions.

Quenching of NBD Emission by Lipophilic Quenching Agents. The membrane location and topography of residues K189−N218 were confirmed by using fluorescence quenching agents that are themselves restricted in location to the nonpolar interior of the membrane. We chose to use 7-doxyl-labeled phosphatidylcholine as the lipophilic quenching reagent because the nitroxide moiety that serves as the quencher is positioned approximately in the middle of each leaflet of the bilayer. However, because of the flexibility and dynamic motion of the acyl chain, all of the NBD probes facing the bilayer will contact the nitroxide moiety and will be quenched, though to different extents.

Nitroxide quenching curves for four NBD-labeled PFO mutants are shown in Figure 5A. The NBD probes attached to residues A195 and N197 are not quenched by the doxyl phospholipid. The lack of contact between these probes and the nitroxide is consistent with the observation that both of these NBD probes have short lifetimes (Figure 3B), are efficiently quenched by the polar collisional quencher I^- (Figure 4B), and hence face the aqueous pore. In contrast, probes positioned in place of the alternate residues, S194 and L196, are quenched by the nitroxide, but not by iodide ions (Figure 4B), a result consistent with the location of these

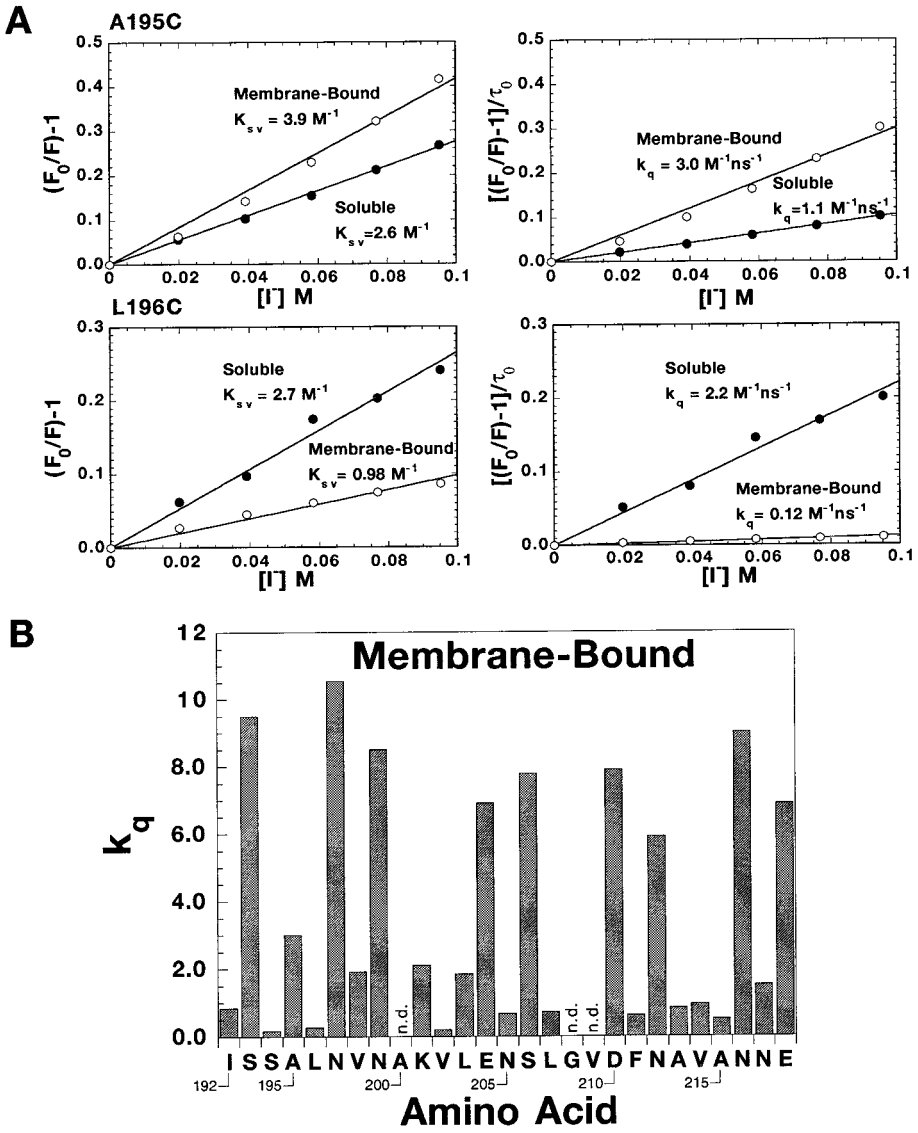

FIGURE 4: Collisional quenching of NBD-labeled mutants of PFO by iodide ions. Exposure of the NBD probes to collisional quenching by iodide ions in the aqueous medium was evaluated using both the Stern−Volmer and bimolecular quenching plots (see the text and Experimental Procedures). The Stern−Volmer plots of the I^- quenching data are shown for both NBD−PFO^{A195C} and NBD−PFO^{L196C} on the left side of panel A, while the right side shows the data after correcting for (dividing by) the unquenched fluorescence lifetime of the NBD probe (τ_o) in the soluble monomer or membrane-bound state as appropriate. In the latter case, the slope of the line yields the bimolecular quenching constant, k_q, instead of the Stern−Volmer constant, K_{sv}. The histogram in panel B shows the k_q value of iodide ions with the membrane-bound form of each NBD-labeled residue in this region. Soluble PFO (●) and membrane-bound PFO (○). n.d. means not determined. Every fifth amino acid is labeled with its primary sequence number on the *X*-axis in the bar chart in panel B.

side chains in the nonpolar interior of the bilayer when PFO is inserted in the membrane. The nonlinearity of these quenching curves shows that nitroxide contact with the NBD is more complicated than a simple collisional model, and nitroxide-dependent fluorescence lifetime measurements reveal that both static quenching and collisional quenching are involved (data not shown). However, the critical issue is not the mechanism of quenching, but rather whether there is quenching.

The sensitivities of the NBD-labeled PFO mutants to the lipophilic quencher are summarized in Figure 5B by comparing the extents of quenching when 20 mol % of the phospholipid is nitroxide-labeled. It is clear from these data that every other residue contacts the phospholipid quencher. The alternating pattern of doxyl quenching, and thus of PFO residues facing the hydrophobic core of the bilayer, therefore demonstrates that residues 192−215 of PFO form an antiparallel amphipathic β-sheet to create the aqueous pore.

One result of the doxyl quenching experiments is particularly interesting, that of NBD−PFO^{I192C}. As shown in Table 1, PFO^{I192C} loses approximately 99% of its hemolytic activity when the cysteine-substituted mutant is derivatized with NBD. One might therefore anticipate that this NBD-labeled mutant would not bind to a membrane. Yet this NBD-labeled residue is quenched by the doxyl phospholipid, and the lifetime results show that this NBD is in a single environment when exposed to liposomes, an environment different than that of the monomer. These data therefore argue strongly that this residue is indeed inserting into the membrane. Thus, we conclude that NBD−PFO^{I192C} is fully insertion-competent, and that its hemolytic activity is blocked at a step after membrane insertion.

DISCUSSION

These studies have demonstrated that upon PFO binding to and insertion into a membrane, a 30-residue stretch of

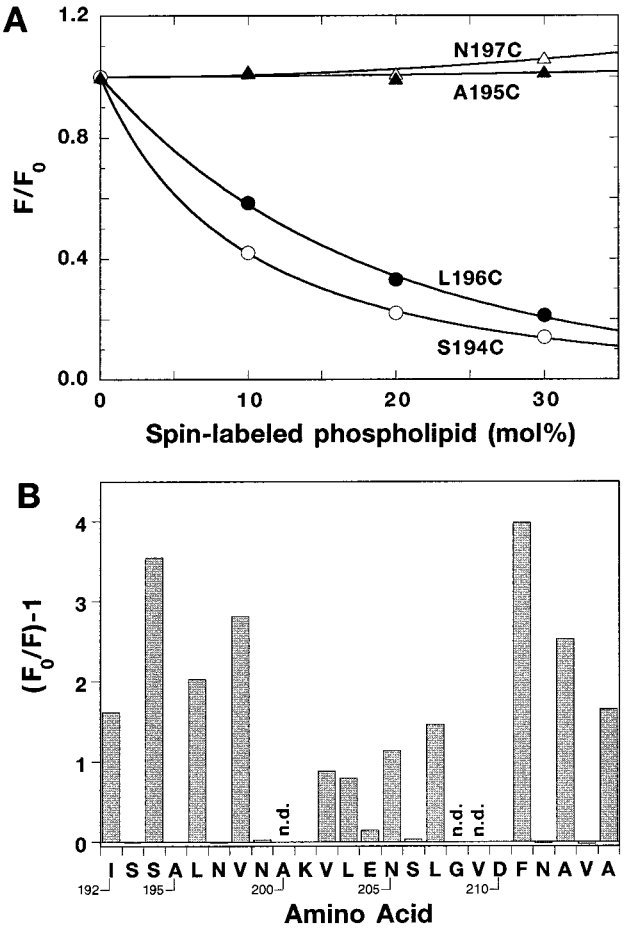

FIGURE 5: Quenching of NBD-labeled mutants of PFO by nitroxide-labeled phospholipid incorporated into liposomes. In panel A, the emission intensities are shown for NBD linked to two cysteine-substituted membrane-facing residues, S194 and L196, and to two channel-facing residues, A195 and N197, as a function of the mol % of the nitroxide-labeled phospholipid in the liposomes. Both membrane-facing NBD residues in the membrane-bound PFO were quenched by the 7-doxyl moiety in a concentration-dependent manner, whereas the residues predicted to face the channel were not quenched by the lipophilic quenching agents in the bilayer. The quenching results for each membrane-bound NBD-substituted mutant are shown in panel B in liposomes containing 20 mol % of the 7-doxyl phospholipid. The symbols shown in panel A are larger than the uncertainty associated with repeated measurements, and in panel B, the replicate measurements were within 3% for those samples that exhibited significant quenching. n.d. means not determined. Every fifth amino acid is labeled with its primary sequence number on the *X*-axis in the bar chart in panel B.

PFO enters the bilayer and spans the membrane as a two-stranded amphipathic β-sheet. The aqueous pore is therefore presumably formed by the hydrogen bonding of double-stranded β-sheets from multiple PFO monomers that results in the creation of a β-barrel that lines the aqueous pore through the bilayer, similar to that shown for the unrelated cytolysin, *Staphylococcus aureus* α-hemolysin (*6*). Interestingly, this stretch of PFO packs as three short α-helices in domain 3 of the soluble PFO monomer crystal structure (Figure 6) (*4*). The transition of this region from a tightly packed α-helical structure in the monomeric form of PFO to an extended β-sheet in the membrane-bound form is the first description of this type of structural transition for a membrane-spanning domain of a toxin.

The trigger(s) for these remarkable changes in secondary and tertiary structure during membrane insertion remains

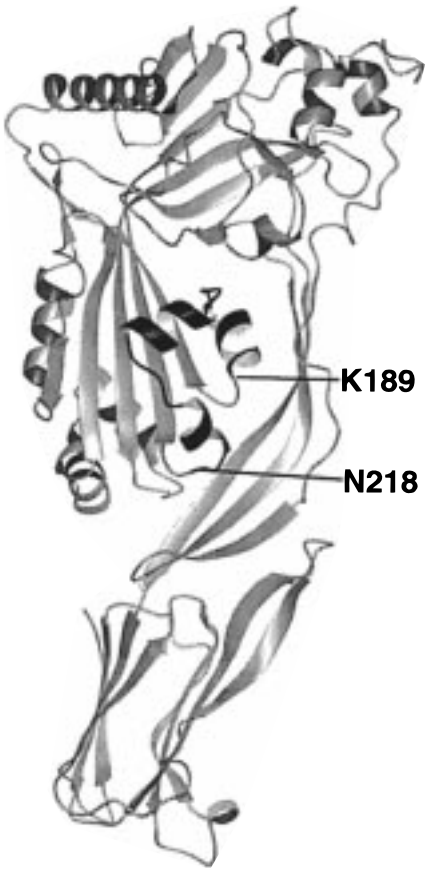

FIGURE 6: Location of the transmembrane domain in the structure of PFO. The ribbon representation of the α-carbon backbone of the PFO crystal structure of the soluble monomer of PFO is shown. The location of the three short α-helices which comprise residues K189−N218 is highlighted in black.

unknown. Low pH triggers membrane insertion for many toxins, as is the case for diphtheria toxin (*24*) and other A−B toxins which transport their catalytic A fragments across an endosomal membrane. However, a similar trigger cannot be invoked for PFO or other pore-forming toxins because their primary target is the plasma membrane. Several pore-forming toxins oligomerize into prepore complexes on the membrane (*19*, *25*, *26*), and it has been hypothesized that oligomerization of such pore-forming toxins induces the conformational changes needed in the monomers to form a preinsertion β-barrel that ultimately inserts spontaneously into the bilayer. However, the precise nature of the interactions between the preinsertion β-barrel and the membrane is unclear.

The data presented here do not yet prove that PFO forms a preinsertion β-barrel, and in fact the combined functional and spectral data suggest that single monomers can insert into the membrane successfully. We have observed a membrane-dependent conformational change in one of our NBD−PFO monomers, NBD−PFO^{I192C}, that suggests insertion may occur prior to formation of the cytolytic complex. Whereas PFO^{I192C} retained 100% of the hemolytic activity of the parent toxin, modification of the substituted cysteine with NBD resulted in the loss of >99% of its hemolytic activity. This loss in hemolytic activity did not appear to result from an inability of the NBD-labeled protein to insert into the bilayer. Fluorescence lifetime data showed that all of the probes in the NBD−PFO^{I192C} sample entered an

environment of intermediate hydrophobicity when exposed to membranes, consistent with its location at the beginning of one of the membrane-penetrating β-sheets. The NBD on PFO^{I192C} was also quenched by nitroxide moieties attached to phospholipid acyl chains, thereby demonstrating that the probes were exposed to the nonpolar core of the bilayer. Finally, the magnitude of the increase in the tryptophan emission of NBD−PFO^{I192C} (as well as the rest of the NBD-derivatized mutants) (data not shown) in the presence of liposomes was similar to that which has been reported to occur when native PFO binds and inserts into the membrane (*23*). The NBD−Cys at the I192 location is therefore inserted into the membrane, but the protein is hemolytically inactive. These results indicate that a step after I192 insertion may be blocked by the NBD modification of PFO^{I192C}, possibly oligomerization. This putative mechanism, that of inserting into the bilayer prior to oligomerization, differs from those described for *S. aureus* α-toxin (*6*), *Clostridium septicum* α-toxin (*26*), and *Aeromonas hydrophila* aerolysin (*25*), in which a fully oligomerized complex forms prior to membrane insertion. Palmer et al. (*27*) have suggested that dimers of streptolysin O, a toxin related to PFO, may also insert into the membrane prior to the assembly of a complete oligomer. If single molecules of PFO insert, then this mechanism would suggest that the association of a single PFO molecule (and presumably related toxins) with the membrane can elicit major conformational changes in their structure. We are currently pursuing this intriguing possibility.

Is this region the only membrane-spanning region of PFO? It is clear that domain 4 (carboxyl-terminal residues 390−500), which contains the membrane-binding domain (*28*−*30*), must also interact with the membrane surface. Sekino-Suzuki et al. (*30*) have shown that tryptophan residues in domain 4 of PFO undergo a significant increase in emission intensity when bound to cholesterol-containing liposomes, and we have confirmed this observation (data not shown). Also, Nakamura et al. (*23*) have shown that some or all of these tryptophans could be collisionally quenched in a nonoligomerizing, cytolytically inactive derivative of PFO, MCθ, by brominated phosphatidylcholine−cholesterol membranes. This observation indicates that some of the tryptophans in domain 4 are exposed to membrane lipids, although the extent to which domain 4 penetrates the membrane remains unclear. Thus, the nature of the interaction between PFO domain 4 and the membrane remains to be elucidated, as does the possibility of other membrane-interactive sequences in PFO.

Recently, Palmer et al. (*7*) suggested that residues 274−307 of SLO comprised its membrane-interactive region and formed two amphipathic α-helices. These SLO residues align with residues L203−V233 of PFO, half of which are positioned in the interior of the PFO monomer crystal structure (*4*). However, we have shown in this study, by a combination of spectroscopic techniques, that PFO contains an overlapping domain that encompasses residues K189−N218 and that PFO interacts with the membrane via a two-stranded amphipathic β-sheet structure rather than via a pair of amphipathic α-helices. The amphipathic β-sheet motif is reproduced in all of the known primary structures of related thiol-activated toxins, including SLO (Figure 1). Furthermore, the region suggested by Palmer et al. to be the membrane-penetrating domain of SLO could not be modeled as a pair of amphipathic α-helices in PFO. The region identified by Palmer et al. corresponds partly to a central β-strand of domain 3, and it is unlikely that a core β-strand of domain 3 could be disrupted to form an amphiphilic segment during membrane binding. Thus, we predict that all members of the thiol-activated toxin family, including SLO, interact with the membrane via the structural region which approximately correspond to residues K189−N218 of PFO.

In addition to defining a membrane-spanning region of PFO, we have also demonstrated the usefulness of NBD fluorescence for these types of analyses. By measuring several different independent parameters, we have been able to obtain a more detailed picture of the monomer-to-oligomer transition than previously possible. Furthermore, the combination of the independent data from each type of analysis shown here has eliminated much of the ambiguity associated with single-technique intensity measurements. The lifetime measurements were particularly useful because they allowed us not only to detect and identify the environment of each probe in the sample but also to quantify the fraction of NBD dyes in each environment, both before and after membrane insertion of PFO. Of particular importance, this approach allowed us to show that our samples were homogeneous and that each of the NBD-labeled PFO proteins in a sample underwent the same transition during membrane insertion. Such quantitative data cannot be elicited from the measurement of wavelength shifts in the emission or intensity changes, as noted above in the Results. To date, acrylodan has been used to assess environmental polarity because of the large blue shift it experiences in moving from a polar to a nonpolar milieu. However, acrylodan is so hydrophobic that it has a tendency to insert itself into a bilayer even when the dye is predicted to be located on the hydrophilic face of the amphipathic β-sheet in the pore in artificial bilayers (*19*), though not in natural bilayers (*31*). In contrast, we have shown here that NBD is well-behaved in both nonpolar and aqueous environments, in liposomes or natural membranes. Thus, this approach, using a combination of fluorescent techniques with NBD dyes, provides a reliable means of identifying transmembrane domains and their conformations within the bilayer. In addition, other types of interactions and conformational changes that occur during the transition of toxins from soluble monomers to membrane-bound complexes can be characterized using these spectroscopic techniques.

ACKNOWLEDGMENT

We acknowledge the excellent technical support of Amy Marpoe, Marianne Rogers, and Angela Maupin. We thank Susanne Feil, William McKinstry, and Galina Polekhina for their important contributions to our structural studies of PFO.

REFERENCES

1. Tweten, R. K. (1995) in *Virulence Mechanisms of Bacterial Pathogens* (Roth, J. A., Bolin, C. A., Brogden, K. A., Minion, C., and Wannemuehler, M. J., Eds.) pp 207−230, American Society for Microbiology, Washington, DC.
2. Billington, S. J., Jost, B. H., Cuevas, W. A., Bright, K. R., and Songer, J. G. (1997) *J. Bacteriol. 179*, 6100−6106.

3. Olofsson, A., Hebert, H., and Thelestam, M. (1993) *FEBS Lett. 319*, 125−127.
4. Rossjohn, J., Feil, S. C., McKinstry, W. J., Tweten, R. K., and Parker, M. W. (1997) *Cell 89*, 685−692.
5. Oh, K. J., Zhan, H., Cui, C., Hideg, K., Collier, R. J., and Hubbell, W. L. (1996) *Science 273*, 810−812.
6. Song, L. Z., Hobaugh, M. R., Shustak, C., Cheley, S., Bayley, H., and Gouaux, J. E. (1996) *Science 274*, 1859−1866.
7. Palmer, M., Saweljew, P., Vulicevic, I., Valeva, A., Kehoe, M., and Bhakdi, S. (1996) *J. Biol. Chem. 271*, 26664−26667.
8. Ho, S. N., Hunt, H. D., Horton, R. M., Pullen, J. K., and Pease, L. R. (1989) *Gene 77*, 51−59.
9. Sambrook, J., Fritsch, E., and Maniatis, T. (1989) *Molecular Cloning; A Laboratory Manual*, Cold Spring Harbor Laboratory Press, Cold Spring Harbor, NY.
10. Haugland, R. P. (1996) *Handbook of fluorescent probes and research chemicals*, 6th ed., Molecular Probes, Inc., Eugene, OR.
11. MacDonald, R. C., MacDonald, R. I., Menco, B. P. M., Takeshita, K., Subbarao, N. K., and Hu, L.-R. (1991) *Biochim. Biophys. Acta 1061*, 297−303.
12. Harris, R. W., Sims, P. J., and Tweten, R. K. (1991) *J. Biol. Chem. 266*, 6936−6941.
13. Ye, J., Esmon, N. L., Esmon, C. T., and Johnson, A. E. (1991) *J. Biol. Chem. 266*, 23016−23021.
14. Dell, V. A., Miller, D. L., and Johnson, A. E. (1990) *Biochemistry 29*, 1757−1763.
15. Spencer, R. D., and Weber, G. (1970) *J. Chem. Phys. 52*, 1654−1663.
16. Alcala, J. R., Gratton, E., and Prendergast, F. G. (1987) *Biophys. J. 51*, 587−596.
17. Crowley, K. S., Reinhart, G. D., and Johnson, A. E. (1993) *Cell 73*, 1101−1115.
18. Crowley, K. S., Liao, S., Worrell, V. E., Reinhart, G. D., and Johnson, A. E. (1994) *Cell 78*, 461−471.
19. Valeva, A., Weisser, A., Walker, B., Kehoe, M., Bayley, H., Bhakdi, S., and Palmer, M. (1996) *EMBO J. 15*, 1857−1864.
20. Cowan, S. W., and Rosenbusch, J. P. (1994) *Science 264*, 914−916.
21. Saunders, K. F., Mitchell, T. J., Walker, J. A., Andrew, P. W., and Boulnois, G. J. (1989) *Infect. Immun. 57*, 2547−2552.
22. Pinkney, M., Beachey, E., and Kehoe, M. (1989) *Infect. Immun. 57*, 2553−2558.
23. Nakamura, M., Sekino, N., Iwamoto, M., and Ohno-Iwashita, Y. (1995) *Biochemistry 34*, 6513−6520.
24. Blewitt, M. G., Chung, L. A., and London, E. (1985) *Biochemistry 24*, 5458−5464.
25. Van der Goot, F. G., Pattus, F., Wong, K. R., and Buckley, J. T. (1993) *Biochemistry 32*, 2636−2642.
26. Sellman, B. R., Kagan, B. L., and Tweten, R. K. (1997) *Mol. Microbiol. 23*, 551−558.
27. Palmer, M., Harris, R., Freytag, C., Kehoe, M., Tranum-Jensen, J., and Bhakdi, S. (1998) *EMBO J. 17*, 1598−1605.
28. Tweten, R. K., Harris, R. W., and Sims, P. J. (1991) *J. Biol. Chem. 266*, 12449−12454.
29. Iwamoto, M., Ohno-Iwashita, Y., and Ando, S. (1990) *Eur. J. Biochem. 194*, 25−31.
30. Sekino-Suzuki, N., Nakamura, M., Mitsui, K. I., and Ohno-Iwashita, Y. (1996) *Eur. J. Biochem. 241*, 941−947.
31. Valeva, A., Walev, I., Pinkernell, M., Walker, B., Bayley, H., Palmer, M., and Bhakdi, S. (1997) *Proc. Natl. Acad. Sci. U.S.A. 94*, 11607−11611.

BI981452F